Study of the Recombination Reaction $CCl_3 + O_2$ (+M) → CCl_3O_2 (+M) at Pressures of 2−900 bar and Temperatures of 260−346 K†

Klaus Luther,* Kawon Oum, and Jürgen Troe

Institut für Physikalische Chemie, Universität Göttingen, Tammannstrasse 6, D-37077 Göttingen, Germany

Received: October 19, 2000; In Final Form: December 5, 2000

The recombination reaction $CCl_3 + O_2$ (+M) → CCl_3O_2 (+M) was studied in the upper part of the falloff curve at 260, 300, and 346 K over the pressure range of 2−900 bar. CCl_3 radicals were generated by photolysis of CCl_3Br at 248 nm; the temporal decay of the absorption from CCl_3 at 223.5 nm was monitored in the presence of O_2; falloff curves of the rate constants were determined in N_2 and He as bath gases. The falloff curves could well be represented by limiting high-pressure rate constants $k_\infty = (5.2 \pm 0.2) \times 10^{-12}$ $(T/300\ \mathrm{K})^{-1.4\pm0.4}$ cm^3 molecule^{-1} s^{-1} from the present work, limiting low-pressure rate constants $k_0 = [N_2]\ (1.1 \pm 0.3) \times 10^{-30}$ $(T/300\ \mathrm{K})^{-6.3\pm1.0}$ cm^3 molecule^{-1} s^{-1} or $k_0 = [\mathrm{He}]\ (4.2 \pm 0.7) \times 10^{-31}$ $(T/300\ \mathrm{K})^{-6.9\pm1.0}$ cm^3 molecule^{-1} s^{-1} from the literature, and center-broadening factors $F_c\ (N_2) = (0.35 \pm 0.03)$ $(T/300\ \mathrm{K})^{-0.35}$ or $F_c\ (\mathrm{He}) = (0.30 \pm 0.03)$ $(T/300\ \mathrm{K})^{-0.48}$ derived from unimolecular rate theory. An onset of diffusion-controlled kinetics at pressures above about 300 bar of N_2 was observed, in agreement with predictions from simple diffusion models. The derived rate constants are analyzed in the framework of unimolecular rate theory.

Introduction

Because of their importance for atmospheric and combustion chemistry, CX_3 radicals (X = H, Cl, F, and combinations) have received much attention. Once CX_3 radicals are formed during the photodegradation of halo(hydro)carbons in the atmosphere, their oxidation with abundant O_2 leads to CX_3O_2.[1,2] Understanding the characteristics of the temperature and pressure dependence of the CX_3 addition reaction with O_2, therefore, is desirable.

Within the series of reactions $CX_3 + O_2$ (+ M) → CX_3O_2 (+ M), with X = H, F, and Cl, the high-pressure rate constants appear to increase in the order of $k(CH_3) < k(CCl_3) < k(CF_3)$,[3] with the small positive temperature coefficient of $k(CH_3)$ suggesting[4] a small activation barrier for the reaction $CH_3 + O_2$ (+ M) → CH_3O_2 (+ M). In contrast to this, the self-recombinations $2CX_3$ (+ M) → C_2X_6 (+ M) seem to have rate constants in the order[5] of $k(CCl_3) < k(CF_3) < k(CH_3)$ without activation barriers. To verify these different trends, more extended studies and confirmations of earlier results are required. The present work provides such investigations for the addition of CCl_3 to O_2.

The reaction $CCl_3 + O_2$ (+ M) → CCl_3O_2 (+ M) has been studied before using the bath gases N_2,[6,7] He,[6,8,9] and Ar[10] and employing pressures in the range of 10^{-3}−1 bar. The rate constants showed the usual falloff behavior of recombination reactions, which corresponds to the mechanism

$$CCl_3 + O_2 \rightleftharpoons CCl_3O_2^*$$

$$CCl_3O_2^* + M \rightarrow CCl_3O_2 + M \qquad (1)$$

However, because the measurements were limited to pressures below 1 bar, they only covered the low-pressure part of the falloff curves. Measurements at elevated temperatures, where back-dissociation of CCl_3O_2 sets in, also allowed us to measure the equilibrium constant of the equilibrium $CCl_3 + O_2 \rightleftharpoons CCl_3O_2$, which led to a reaction enthalpy of[11] $\Delta H^0_{298} = -19.9$ (±0.1) kcal mol^{-1}.

Although the measurements of the falloff curve could be extrapolated relatively well to the low pressure limit, extrapolations to the high-pressure limit remained uncertain because of the restricted experimentally available pressure range. It is this open question which is addressed in the present work, in which we report rate constants of the reaction $CCl_3 + O_2$ (+ M) → CCl_3O_2 (+ M) over the pressure range of 2−900 bar at the temperatures 260, 300, and 346 K.

Experimental Section

In our work, a high-pressure flow cell was employed. CCl_3 radicals were generated by UV laser photolysis, and UV absorption was used for monitoring the temporal loss of the radicals by reaction with O_2. Our experimental setup has been described in detail elsewhere[12] and is only briefly characterized here.

A high-pressure cell of 9 mm inner diameter and 10 cm length was used, which allowed us to do experiments at pressures up to 1000 bar and at temperatures between 150 and 500 K. The cell was surrounded by a cooling−heating jacket made of copper tube. Low temperatures were reached by flowing liquid nitrogen through the cooling copper tube, and higher temperatures were obtained by heating a wire inside the tube. Two platinum resistance thermometers were directly attached to the front and backsides of the cell to measure the temperature.

CCl_3 radicals in their ground electronic state were produced by the laser photolysis of CCl_3Br at 248 nm. The laser (Lambda Physik, model LPX 100) operated at 0.2−1 Hz with an output energy of about 200 mJ/pulse. Premixed gas mixtures of the precursor CCl_3Br, O_2, and the bath gas were compressed in an oil-free diaphragm compressor with a double head in parallel-line (Nova Swiss, model 5542321; max operating pressure 1000 bar) and then flowed through the high-pressure cell. Flow rates

† Part of the special issue "Edward W. Schlag Festschrift".

* To whom correspondence should be addressed. Tel: +49 551 39 3120. Fax: +49 551 39 3150; E-mail: kluther@gwdg.de.

10.1021/jp003844d CCC: $20.00
Published on Web 01/31/2001

were controlled by flow meters (Tylan FM361 and FM362) at rates such that reagents and products were removed from the observation volume between laser pulses. Total pressures were measured with high-pressure meters (Burster, model 8201).

UV absorption signals were recorded over a path length of 10 cm. A high-pressure xenon arc lamp (Ushio model UXM 200H; high brightness 200 W) served as the light source. A wavelength of 223.5 nm was chosen for the detection, optimizing the lamp intensity and the absolute and relative values of the absorption cross sections of the CCl_3 radicals and of the products CCl_3O_2 which have overlapping but separable continuous spectra in the UV, see below.

The laser beam and the light of the lamp were conducted collinearly through the high-pressure cell through quartz windows, via a set of laser mirrors (Laser Optik; high reflectance at 248 nm, high transmittance at 220 nm, 45°) in a counterpropagating way. A set of aluminum-coated mirrors directed the lamp light from the cell toward the entrance slit of a monochromator (Zeiss, model MM3)−photomultiplier (Hamamatsu, model R106) arrangement. The transient light signals were monitored by a digital oscilloscope (LeCroy, model 9400; band width 125 MHz), averaged over several hundred laser shots, and stored in a microcomputer for further data processing.

Impurities in the bath gases N_2 (Messer-Griesheim, 99.996%) and He (Messer-Griesheim, 99.996%) were removed by a gas cleaning adsorber (Oxisorb, Messer-Griesheim) and dust filters. CCl_3Br (Aldrich, 99.9%) was purified in a pump−thaw−freezing cycle before use. High purity O_2 (MG, 99.996%) was used as received.

Results

CCl_3 radicals in the high-pressure cell were formed by laser photolysis of CCl_3Br at 248 nm

$$CCl_3Br + h\nu\ (248\ nm) \rightarrow CCl_3 + Br \qquad (2)$$

After light absorption at 248 nm, CCl_3Br undergoes C−Br bond fission exclusively and leads to equal amounts of CCl_3 radicals and Br atoms.[13,14] In the presence of O_2, CCl_3 radicals are predominantly removed by the reaction[15]

$$CCl_3 + O_2\ (+ M) \rightarrow CCl_3O_2\ (+ M) \qquad (1)$$

Our observations are fully in accord with this simple reaction mechanism. Figure 1 shows a typical temporal profile of the absorption signal at 223.5 nm, measured at room temperature and in 711 bar of N_2. The signal corresponds to the decay of CCl_3 radicals because of reaction 1 which is followed by the production of CCl_3O_2 via reaction 2. Typical concentrations in our study were $[CCl_3]_0 = (1-10) \times 10^{14}$ molecule cm^{-3} and $[O_2]_0 = (1-10) \times 10^{16}$ molecule cm^{-3} such that pseudo-first-order behavior was reached.

CCl_3O_2 on our time scale was a stable end product. Subsequent reactions removing CCl_3O_2 were too slow to be observed, see below. Despite the simple pseudo-first-order appearance of the observed absorption−time profiles, one has to consider a series of side reactions. In the absence of O_2, e.g., the reactions

$$CCl_3 + Br\ (+ M) \rightarrow CCl_3Br\ (+ M) \qquad (3)$$

$$Br + Br\ (+ M) \rightarrow Br_2\ (+ M) \qquad (4)$$

$$CCl_3 + CCl_3\ (+ M) \rightarrow CCl_3CCl_3\ (+ M) \qquad (5)$$

$$CCl_3 + Br_2 \rightarrow CCl_3Br + Br \qquad (6)$$

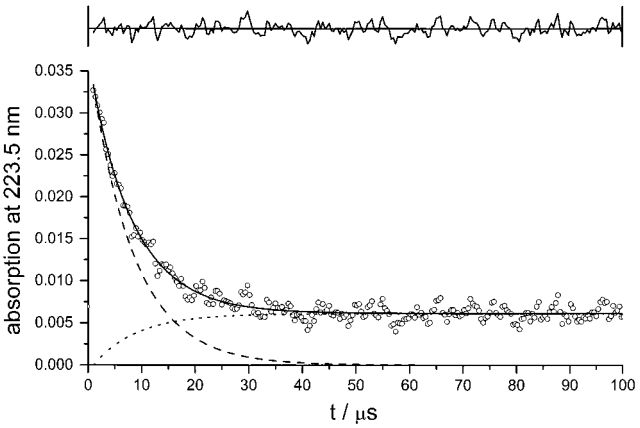

Figure 1. Absorption signal at 223.5 nm recorded after photolysis of CCl_3Br in the presence of O_2 ($[CCl_3]_0 = 4.3 \times 10^{14}$ molecule cm^{-3}, $[O_2]_0 = 3.5 \times 10^{16}$ molecule cm^{-3}, $p(N_2) = 711$ bar, $T = 300$ K; signal averaged over 100 laser shots). Dashed curve, fitted profile of CCl_3; dotted curve, fitted profile for CCl_3O_2; full line, complete fitted absorption signal with residual of the fitting procedure shown on top.

have to be taken into account. We have investigated these reactions up to pressures of 1000 bar in a separate study, whose results will be published soon.[16] Simulations of the mechanism including the observed rate constants clearly show that adding excess O_2 completely suppresses reactions 3−6. On the other hand, addition of Br to O_2 forming BrOO might be considered. However, the reported[17] bond energy of about 4 kJ mol^{-1} is too low to allow for substantial formation of BrOO and possible secondary reactions.

The observed absorption signals approached a steady level after about 50 μs and did not change significantly over about the next 200 μs. A decay of the attained absorption level was observed only on a much longer time being of the order of several milliseconds. In the present work, we did not look into the details of the self-reaction of CCl_3O_2 or the reactions of CCl_3O_2 with Br, because the absorption profiles shown in Figure 1 did not provide any evidence for processes of this type to occur on the short times evaluated in our work.

For pseudo-first-order conditions, the signals of Figure 1 lead directly to the pseudo-first-order rate constant of reaction 1. A simulation on the basis of literature values of the absorption cross sections for CCl_3 ($\sigma = (8-9) \times 10^{-18}$ cm^2 molecule^{-1} from refs 18 and 19) and CCl_3O_2 ($\sigma = 1.6 \times 10^{-18}$ cm^2 molecule^{-1} from refs 11 and 20) allowed for the determination of the quantity of CCl_3 radicals produced and for a check of the extent of the conversion of CCl_3 into CCl_3O_2. The absorption coefficients of C_2Cl_6 ($\sigma \approx 7 \times 10^{-19}$ cm^2 molecule^{-1}) and CCl_3-Br ($\sigma \approx 6 \times 10^{-19}$ cm^2 molecule^{-1}) were measured in our study. No indications of processes other than reactions 1 and 2 were found by this simulation. Including or excluding reactions 3−6 made no difference. The evaluation of Figure 1, therefore, directly led to the rate constant k_1. Figure 1 includes the corresponding CCl_3 and CCl_3O_2 absorption profiles.

Besides measurements near room temperature in Figure 1, Figure 2 shows examples of absorption−time profiles for other O_2 concentrations and other temperatures. Here the concentration effect dominates over a smaller opposite temperature effect, see below. The CCl_3 and CCl_3O_2 contributions are included in the figures, confirming the internal consistency of the evaluation. Tables 1 and 2 summarize the pseudo-second-order rate constants k_1 from our work. Each point corresponds to the average of several hundred measurements, statistical error limits corresponding to 2 σ standard deviations.

TABLE 1: Pseudo-Second-Order Rate Constants k_1 for the Recombination Reaction $CCl_3 + O_2$ (+M) → CCl_3O_2 (+M) at 300 K

M = N_2			M = He		
$p(N_2)$/bar	$[N_2]$/molecule cm^{-3}	$k_1/10^{-12}$ cm^3 molecule^{-1} s^{-1}	p(He)/bar	[He]/molecule cm^{-3}	$k_1/10^{-12}$ cm^3 molecule^{-1} s^{-1}
2	4.89×10^{19}	2.29 ± 0.21	3	7.28×10^{19}	1.68 ± 0.26
3	7.34×10^{19}	2.44 ± 0.37	4	9.70×10^{19}	2.09 ± 0.46
4	9.79×10^{19}	2.51 ± 0.31	6	1.45×10^{20}	2.33 ± 0.58
5	1.22×10^{20}	2.89 ± 0.43	8	1.94×10^{20}	2.57 ± 0.45
6	1.47×10^{20}	3.01 ± 0.86	10	2.42×10^{20}	2.60 ± 1.51
8	1.96×10^{20}	3.18 ± 1.15	12	2.90×10^{20}	2.59 ± 0.77
10	2.45×10^{20}	3.56 ± 2.35	15	3.62×10^{20}	2.63 ± 0.89
20	4.86×10^{20}	3.66 ± 0.74	17	4.10×10^{20}	2.62 ± 0.65
30	7.33×10^{20}	3.87 ± 2.64	19	4.70×10^{20}	2.59 ± 0.67
40	9.80×10^{20}	4.03 ± 1.44	20	4.81×10^{20}	2.78 ± 1.09
60	1.46×10^{21}	3.91 ± 1.60	20	4.81×10^{20}	3.00 ± 0.34
80	1.95×10^{21}	4.09 ± 2.10	30	7.19×10^{20}	3.30 ± 0.95
99	2.41×10^{21}	4.20 ± 2.47	40	9.54×10^{20}	3.49 ± 0.95
204	4.70×10^{21}	3.98 ± 0.69	50	1.19×10^{21}	3.53 ± 1.05
298	6.52×10^{21}	4.19 ± 2.35	60	1.42×10^{21}	3.63 ± 1.21
302	6.61×10^{21}	3.71 ± 2.19	70	1.65×10^{21}	3.67 ± 1.26
304	6.61×10^{21}	4.34 ± 1.21	77	1.81×10^{21}	3.70 ± 1.38
400	7.80×10^{21}	3.66 ± 0.65	99	2.30×10^{21}	3.77 ± 1.57
404	7.86×10^{21}	3.73 ± 0.73	123	2.83×10^{21}	3.94 ± 1.64
503	8.96×10^{21}	3.38 ± 1.25	151	3.43×10^{21}	4.05 ± 1.90
586	9.70×10^{21}	3.22 ± 1.17	209	4.62×10^{21}	4.14 ± 1.20
603	9.87×10^{21}	3.16 ± 1.17	304	6.48×10^{21}	4.06 ± 0.93
706	1.06×10^{22}	2.79 ± 1.16	406	8.30×10^{21}	4.19 ± 1.77
711	1.07×10^{22}	3.19 ± 0.76	506	9.97×10^{21}	4.27 ± 2.31
804	1.13×10^{22}	2.91 ± 0.70	610	1.16×10^{22}	4.25 ± 1.98
892	1.18×10^{22}	3.04 ± 1.90	709	1.30×10^{22}	4.01 ± 1.36
			798	1.43×10^{22}	4.07 ± 1.36

TABLE 2: Pseudo-Second-Order Rate Constants k_1 for the Recombination Reaction $CCl_3 + O_2$ (+He) → CCl_3O_2 (+He) at 260 and 346 K

at 260 K			at 346 K		
p(He)/bar	[He]/molecule cm^{-3}	$k_1/10^{-12}$ cm^3 molecule^{-1} s^{-1}	p(He)/bar	[He]/molecule cm^{-3}	$k_1/10^{-12}$ cm^3 molecule^{-1} s^{-1}
3	8.39×10^{19}	3.41 ± 1.04	3	6.27×10^{19}	1.08 ± 0.15
4	1.13×10^{20}	3.64 ± 0.81	4	8.35×10^{19}	1.13 ± 0.20
6	1.69×10^{20}	3.53 ± 1.92	5	1.04×10^{20}	1.20 ± 0.18
9	2.49×10^{20}	3.89 ± 1.39	6	1.25×10^{20}	1.21 ± 0.20
20	5.51×10^{20}	4.45 ± 2.49	8	1.67×10^{20}	1.39 ± 0.27
30	8.23×10^{20}	4.53 ± 3.18	10	2.08×10^{20}	1.36 ± 0.53
40	1.09×10^{21}	5.42 ± 1.73	12	2.50×10^{20}	1.79 ± 0.96
60	1.62×10^{21}	5.09 ± 2.04	20	4.16×10^{20}	2.09 ± 0.37
70	1.88×10^{21}	5.39 ± 1.49	30	6.19×10^{20}	2.02 ± 0.60
80	2.14×10^{21}	5.13 ± 1.02	40	8.23×10^{20}	2.11 ± 0.71
113	2.97×10^{21}	5.67 ± 2.43	57	1.17×10^{21}	2.50 ± 1.03
305	7.31×10^{21}	5.78 ± 1.08	79	1.60×10^{21}	2.62 ± 1.33
407	9.33×10^{21}	4.99 ± 1.23	99	2.00×10^{21}	2.80 ± 1.71
509	1.12×10^{22}	5.09 ± 1.03	206	3.99×10^{21}	2.75 ± 0.86
605	1.28×10^{22}	5.04 ± 1.83	299	5.59×10^{21}	2.97 ± 1.05
699	1.43×10^{22}	4.69 ± 1.69	405	7.28×10^{21}	2.98 ± 1.25
799	1.57×10^{22}	5.44 ± 2.58	501	8.70×10^{21}	3.15 ± 0.86
			599	1.01×10^{22}	3.13 ± 1.54
			701	1.15×10^{22}	3.20 ± 1.69
			815	1.29×10^{22}	3.11 ± 2.02

Figure 3 illustrates the pressure dependence of k_1 at temperatures near 300 K and for the bath gases He and N_2. To represent the full falloff curve, our data at high pressures are combined with the previous low-pressure measurements from refs 6−9. The typical falloff behavior of a recombination reaction is observed with a smooth transition from the limiting low-pressure rate constant $k_{1,0}$ to the limiting high-pressure rate constant $k_{1,\infty}$.

Figure 4, for the bath gas He, compares our rate constants at 300 K with the results for 260 and 346 K. There is a clear indication of a negative temperature coefficient near to the high-pressure limit which cannot be attributed to the common shift of the center of the falloff curves toward high pressures when the temperature is increased. No indications for an onset of diffusion control are observed in helium even at the highest pressures. In contrast to this, diffusional effects are becoming visible at the highest pressures in the bath gas N_2, see Figure 3 and enlarged in Figure 5. These effects, however, can clearly be separated such that they do not influence our falloff extrapolations.

Our measurements alone are well-suited for extrapolations to the limiting high-pressure rate constants $k_{1,\infty}$, whereas their extrapolation to the limiting low-pressure rate constants $k_{1,0}$ leaves a much larger uncertainty. We, therefore, combine our data with the earlier low-pressure measurements from refs 6−9 which improves our high-pressure extrapolation. On the other hand, combining the measurements from refs 6−9 with the present results allows for a better specification of low-pressure falloff corrections to the data from refs 6−9. For the combined

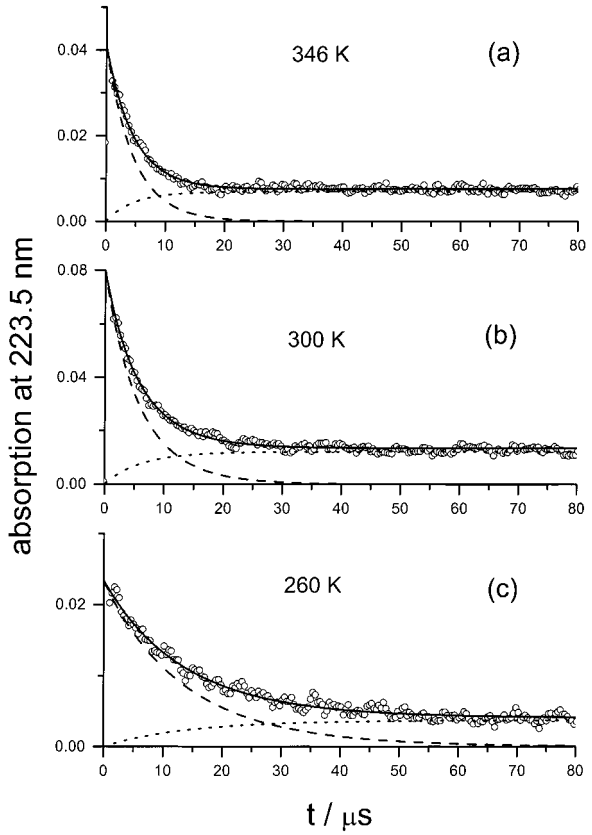

Figure 2. Same as Figure 1 for the bath gas He at 346 K (top), 300 K (middle), and 260 K (bottom) and p(He) ≈ 700 bar (experimental conditions: (a) $[O_2]_0 = 6.2 \times 10^{16}$ molecule cm^{-3}, $[CCl_3]_0 = 4.6 \times 10^{14}$ molecule cm^{-3}, p(He) = 701 bar; (b) $[O_2]_0 = 3.4 \times 10^{16}$ molecule cm^{-3}, $[CCl_3]_0 = 9.1 \times 10^{14}$ molecule cm^{-3}, p(He) = 709 bar; (c) $[O_2]_0 = 1.3 \times 10^{16}$ molecule cm^{-3}, $[CCl_3]_0 = 2.6 \times 10^{14}$ molecule cm^{-3}, p(He) = 699 bar).

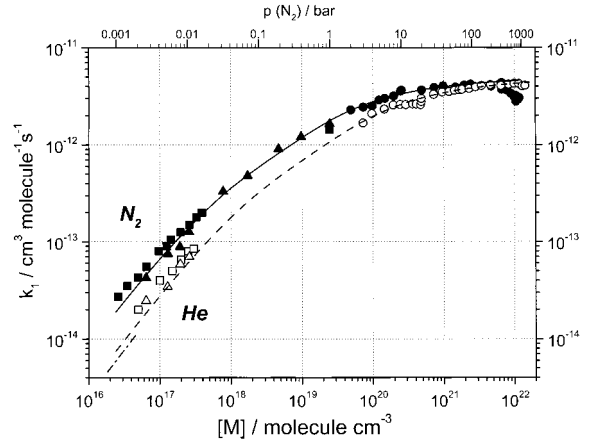

Figure 3. Falloff curves for the recombination reaction $CCl_3 + O_2$ (+ M) → CCl_3O_2 (+ M) at 300 K, with measurements in the bath gases N_2 (filled symbols) and He (open symbols). Circles: this work. Triangles: experiments by Fenter et al. (ref 6). Filled squares: experiments by Danis et al. in N_2 (ref 7). Open squares: experiments by Ryan and Plumb in He (ref 9). Dashed−dotted line: data from Nottingham et al. in He (ref 8). Dashed and full lines: falloff representations of this work, see text.

representation of all data, we use the standard form of falloff curves from refs 21−23:

$$\frac{k_1}{k_{1,\infty}} \approx \left\{\frac{X}{1+X}\right\} F_c^{\{1+[\log(X)/(0.75-1.27\log(F_c))]^2\}^{-1}} \quad (7)$$

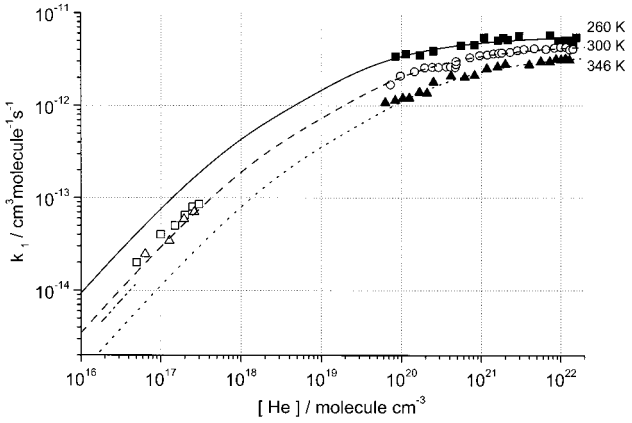

Figure 4. Falloff curves for the bath gas He at $T = 260$ (■), 300 (○), and 346 K (▲) from this work. The low-pressure data at 300 K were obtained by Fenter et al. (△; ref 6) and by Ryan and Plumb (□; ref 9). Dashed−dotted line: data from Nottingham et al. (ref 8) at room temperature. The lines correspond to the falloff representation from this work, see text.

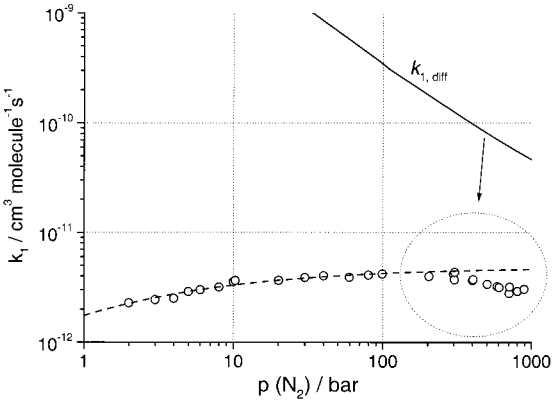

Figure 5. Falloff curve in the bath gas N_2 at 300 K showing the onset of the diffusion control. The decline of the rate constants at pressures over 300 bar is emphasized by the encircled area. Rate constants for fully diffusion-controlled recombination, such as those calculated in the text, are shown as a solid line at the top. The dashed line corresponds to the falloff representation without considering diffusional effects, see text.

with $X = k_{1,0}/k_{1,\infty}$. The limiting pseudo-second-order low-pressure rate constant $k_{1,0}$ is proportional to the bath gas concentration [M]. F_c denotes the center-broadening factor of the falloff curve; a value of $F_c = 1$ would correspond to the Lindemann−Hinshelwood model of unimolecular rate theory. A Levenberg−Marquardt least-squares fit of all data to eq 7 leads to the following values of $k_{1,\infty}$, $k_{1,0}$, and F_c:

$$k_{1,\infty} = (5.2 \pm 0.2) \times 10^{-12} (T/300\ \mathrm{K})^{-1.4\pm0.4}\ \mathrm{cm^3\ molecule^{-1}\ s^{-1}} \quad (8)$$

$$k_{1,0} = [\mathrm{N_2}]\ (1.1 \pm 0.3) \times 10^{-30} (T/300\ \mathrm{K})^{-6.3\pm1.0}\ \mathrm{cm^3\ molecule^{-1}\ s^{-1}} \quad (9)$$

$$k_{1,0} = [\mathrm{He}]\ (4.2 \pm 0.7) \times 10^{-31} (T/300\ \mathrm{K})^{-6.9\pm1.0}\ \mathrm{cm^3\ molecule^{-1}\ s^{-1}} \quad (10)$$

$$F_c(\mathrm{N_2}, 300\ \mathrm{K}) = (0.36 \pm 0.03) \quad (11)$$

$$F_c(\mathrm{He}, T) = (0.31 \pm 0.03)\ (T/300\ \mathrm{K})^{-0.5} \quad (12)$$

The given error limits are based on the scatter of data and on the estimate of possible systematic errors. The fitting results

TABLE 3: Summary of Rate Constants k_1[a]

reference	M	p/bar	$k_{1,0}$/cm^3 molecule^{-1} s^{-1}	$k_{1,\infty}$/cm^3 molecule^{-1} s^{-1}	F_c
6	N_2	$10^{-3}-1$	$(6.9 \pm 0.2)\times10^{-31}$ $(T/300\ K)^{-6.4\pm0.3}$ [M]	$[(2.4 \pm 0.2) \times 10^{-12}$ $(T/300\ K)^{-2.1}]$	0.6
			$(9.5 \pm 0.3) \times 10^{-31}$ $(T/300\ K)^{-6.3\pm0.3}$ [M]	$[(5.8 \pm 0.4) \times 10^{-12}$ $(T/300\ K)^{-0.6}]$	0.3
7	N_2	$(1-16) \times 10^{-3}$ and 1	$(1.6 \pm 0.3) \times 10^{-30}$ $(T/298\ K)^{-6.3\pm0.5}$ [M]	$[(3.2 \pm 0.7) \times 10^{-12}$ $(T/298\ K)^{-1.2}]$	0.3
8	He	$(0.5-2) \times 10^{-3}$	$(2.7 \pm 0.2) \times 10^{-31}$ $(T/300\ K)^{-8.7\pm1.0}$ [M]		
9	He	$(1-11) \times 10^{-3}$	$(5.8 \pm 0.6) \times 10^{-31}$ [M]		
10	Ar	0.97		$[5.1 \times 10^{-12}]$	
this work	N_2	2−900	$[(1.1 \pm 0.3) \times 10^{-30}$ $(T/300\ K)^{-6.3\pm1.0}$ [M]]	$(5.2 \pm 0.2) \times 10^{-12}$ $(T/300\ K)^{-1.4\pm0.4}$	(0.35 ± 0.03) $(T/300\ K)^{-0.35}$
	He	2−900	$[(4.2 \pm 0.7) \times 10^{-31}$ $(T/300\ K)^{-6.9\pm1.0}$ [M]]	$(5.2 \pm 0.2) \times 10^{-12}$ $(T/300\ K)^{-1.4\pm0.4}$	(0.30 ± 0.03) $(T/300\ K)^{-0.48}$

[a] Data in brackets: estimates from falloff extrapolations based on the indicated center-broadening factors F_c, see text.

are shown as lines in Figures 3 and 4. Our present results in Table 3 are compared with earlier data. One should note that falloff extrapolations toward $k_{1,0}$ and $k_{1,\infty}$ may depend on the used values of F_c such that only values derived with similar values of F_c can be compared.

Discussion

Limiting High-Pressure Rate Constants $k_{1,\infty}$. Our present measurements near to the high-pressure limit allow for a meaningful extrapolation to the high-pressure limit. This extrapolation was much less certain on the basis of measurements below 1 bar, although similar values of $k_{1,\infty}$ were obtained from the extrapolations of refs 6 and 7 when similar values of F_c were assumed such as derived from unimolecular rate theory (see Table 3 and ref 24). Assuming a "standard value" of $F_c = 0.6$ underestimates $k_{1,\infty}$ clearly.[25] The present work derived F_c from a fit of the full falloff curves in good agreement with that of the theory, see below.

We have compared our measured values of $k_{1,\infty}$ from eq 8 with theoretical values from the classical trajectory/statistical adiabatic channel calculations for a standard valence potential from ref 26. Without going into the details of these calculations, we report our results of $k_{1,\infty} = 3.8 \times 10^{-12}$ $(T/300\ K)^{+0.41}$ cm^3 molecule^{-1} s^{-1} such as calculated in the available approximation of the potential for a linear + linear fragment → nonlinear adduct reaction with an adduct angle which corresponds to real CCl_3O_2. Neither the calculated small positive temperature coefficient nor the absolute value of $k_{1,\infty}$ agree too well with the measurements. We, therefore, have to conclude that the standard valence potential from ref 26 is too simple to account for finer details of the measurements, although the calculated absolute value of $k_{1,\infty}$ is not too far from the measurements. Manipulating the apparent ratio α/β of the potential would not simultaneously bring the absolute value and the temperature coefficient of $k_{1,\infty}$ into agreement with those of the experiments. For more details of the treatment, see ref 26. A better theoretical modeling of $k_{1,\infty}$, therefore, has to wait for information about the true potential-energy surface of the reactions.

Limiting Low-Pressure Rate Constants $k_{1,0}$. Our theoretical analysis of $k_{1,0}$ was based on the treatment of refs 21, 27, and 28 with molecular parameters such as those also used in refs 7, 11, and 29. On the basis of the experimental values from eqs 9 and 10, this analysis leads to apparent weak collision efficiencies $\beta_c(N_2) = 0.10$ $(T/300\ K)^{-1.5\pm1.0}$ and $\beta_c(He) = 0.03$ $(T/300\ K)^{-2.3\pm1.0}$, or apparent average energies transferred per collision, $-\langle\Delta E\rangle = 40$ $(T/300\ K)^{-0.7\pm1.0}$ cm^{-1} for M = N_2 and $-\langle\Delta E\rangle = 11$ $(T/300\ K)^{-1.4\pm1.0}$ cm^{-1} for M = He. These absolute values of $\langle\Delta E\rangle$ appear rather low. However, they are probably not unreasonable in view of the low bond energy of CCl_3O_2. The standard assumption of nearly temperature independent $\langle\Delta E\rangle$ within the experimental uncertainty is approximately confirmed, although both observed negative temperature coefficients appear to be on the high side. We do not go into more details here but we note that, within the uncertainty of the evaluation, the experimental values of $k_{1,0}$ appear consistent with those of our theoretical analysis.

Center-Broadening Factors F_c. The center-broadening factors F_c play an important role in the evaluation of the experimental falloff curves. If one aims at a description of the full range of pressure dependence it appears not satisfactory to assume a standard value of $F_c = 0.6$, which may be sufficient to reproduce a limited part of the falloff curve but unavoidably leads to erroneous extrapolated limiting rate constants when the true F_c differs from 0.6 and only limited parts of the falloff curve are experimentally accessible. To estimate F_c from theory, we have followed the approach described in refs 21−23. In this treatment, the internal energy $U^{\ddagger}_{vib}$ of the activated complex (excluding external rotations) was identified with the sum of the thermal rovibrational energies of CCl_3 and O_2, which leads to strong collision broadening factors $F_c^{SC} = 0.49$ $(T/300\ K)^{-0.14}$. From the weak collision efficiencies β_c derived in the previous subsection, one obtains[23] $F_c^{WC} = 0.73$ $(T/300\ K)^{-0.22}$ for M = N_2 and $F_c^{WC} = 0.62$ $(T/300\ K)^{-0.34}$ for M = He. Combining F_c^{SC} and F_c^{WC} leads to theoretical estimates of

$$F_c(N_2) = (0.35 \pm 0.03)\ (T/300\ K)^{-0.35} \qquad (13)$$

$$F_c(He) = (0.30 \pm 0.03)\ (T/300\ K)^{-0.48} \qquad (14)$$

which is in remarkably good agreement with the experimentally fitted values given in eqs 11 and 12. Our evaluation of the experimental falloff curve, therefore, appears fully consistent with that of the unimolecular rate theory.

High-Pressure Transition to Diffusion-Controlled Kinetics. Our rate measurements in N_2 at 300−900 bar provide evidence for a transition to diffusion-controlled kinetics. As seen in Figures 3 and 5 (emphasized by the encircled area), the recombination rate constants k_1 for N_2 were found to decrease with increasing pressure above 300 bar. In contrast to this, experiments in He did not show a decrease to any significant degree. The observation of decreasing rate constants at increasing pressures can be explained by the onset of diffusion control.

In the following, we try to quantify the transition to diffusion-controlled kinetics. As usual we employ the simplified relation

$$\frac{1}{k_1} = \frac{1}{k_{1,gas}} + \frac{1}{k_{1,diff}} \qquad (15)$$

for the transition of the rate constant k_1 from its hypothetical gas-phase value $k_{1,gas}$ in the absence of diffusive slowdown of the radical association step to the value $k_{1,diff}$ for fully diffusion-controlled association. $k_{1,gas}$ is represented by the falloff curve of the recombination reaction without diffusion and its extrapo-

lation to the (hypothetical) high-pressure limit. $k_{1,\mathrm{diff}}$ is given by Smoluchowski's equation;

$$k_{1,\mathrm{diff}} \approx 4\pi N_A \alpha D\left(\frac{\sigma_{LJ}(CCl_3) + \sigma_{LJ}(O_2)}{2}\right) \qquad (16)$$

Here, D is the diffusion coefficient for relative diffusion of the reacting species, CCl_3 and O_2, taken as the sum of the individual diffusion coefficients, $D = D(CCl_3-N_2) + D(O_2-N_2)$ in the bath gas N_2. The effective capture distance is estimated as the mean of the Lennard-Jones (LJ) diameters, $\sigma_{LJ}(CCl_3)$ and $\sigma_{LJ}(O_2)$.[30,31] α is the spin statistical factor. We put α equal to $^2/_6$, assuming that all doublet states arising from $^2CCl_3$ and $^3O_2$ in the considered high-density range end up as $^2CCl_3O_2$ in its electronic ground state, whereas all quartet states do not lead to recombination. On the other hand, one should note that we have formulated $k_{1,\mathrm{gas}}$ under the assumption that only the electronic ground state out of the doublet manifold contributes to the gas-phase recombination reaction. Undoubtedly this aspect of the transition between dilute gas and dense fluid recombination requires future refinement.

The specification of the appropriate diffusion coefficient D in eq 16 is not straightforward. For the present situation ($\sigma_{LJ}(CCl_3)/\sigma_{LJ}(N_2) \approx 1.3$, $\sigma_{LJ}(O_2)/\sigma_{LJ}(N_2) = 0.96$, $[N_2] = 10^{21}-10^{22}$ molecule cm^{-3}), the binary diffusion coefficient D_{AM} (A corresponds to the radical and M to N_2) can be derived from an extension of the Stokes−Einstein relation to low pressures. Using refs 32 and 33, D_{AM} is approximated by

$$\frac{kT}{\eta_{N_2} D_{AM}} \approx 3\pi\sigma_{LJ}(CCl_3)\left\{1 - \exp\left(-\frac{[kT/\eta_{N_2} D_{AM}]_0}{3\pi\sigma_{LJ}(CCl_3)}\right)\right\} \qquad (17)$$

where $3\pi\sigma_{LJ}(CCl_3)$ corresponds to the high-density Stokes−Einstein limit of the ratio $kT/\eta_{N_2}D_{AM}$. η_{N_2} denotes the pressure-dependent viscosity of N_2.[33] The low-pressure gas-phase limiting value of D_{AM} is obtained from kinetic gas theory via the Enskog result for diffusion of hard spheres in the gas phase:[32]

$$D^0_{AM} = \frac{3}{8}\frac{1}{\sigma^2_{AM}\Omega\sqrt{\epsilon_A\epsilon_M}[M]}\sqrt{\frac{kTN_A}{2\pi\mu}} \qquad (18)$$

Here, σ is the LJ diameter, ϵ is the LJ well-depth, Ω is the relevant reduced collision integral, and μ is the reduced mass of solvent M and solute A.

The diffusion coefficients, such as calculated above, do not account for strong interactions between the solvent and solutes. A contribution of van der Waals complexes, e.g., in high-pressure gases, may influence the diffusion rates. For example, Terazima and co-workers[34,35] have reported that many radicals diffuse about 2−3 times slower than their parent molecules (depending on the molecular size[34]). The unpaired electron of the radical might cause a larger polarizability because of its extended and diffuse electron cloud which results in a larger friction of the radicals in the solvent because of an attractive intermolecular interaction.[36] The radical−solvent interaction and the resulting local density enhancement around the solute are not reflected in our calculation of the diffusion coefficient; this may imply that our diffusion coefficients for CCl_3 radicals and O_2 in N_2 bath gas may have been overestimated. For more detailed treatments of the diffusional contribution to the recombination rate, see our subsequent articles.[16]

Figure 5 for M = N_2 compares $k_{1,\mathrm{diff}}$ and $k_{1,\mathrm{gas}}$ with the experiments (○). The decline of the recombination rate constants at pressures above 300 bar of N_2 seems to be in line with a transition to diffusion-controlled kinetics, but a possible contribution by the intermolecular solute−solvent interaction is not accounted for. However, this does not affect our main results about the falloff curve, because we did not include the data above 300 bar N_2 in evaluating the limiting high-pressure gas-phase rate constant.

Conclusions

Our experiments provided a considerable extension of the falloff curve of the title reaction by directly measuring the transition to the high-pressure limit. Extrapolations in earlier work from pressures below 1 bar were less reliable in their extrapolation to $k_{1,\infty}$. With the here-derived limiting high-pressure rate constant

$$k_{1,\infty} = (5.2 \pm 0.2) \times 10^{-12} (T/300\ \mathrm{K})^{(-1.4\pm0.4)}\ \mathrm{cm^3\ molecule^{-1}\ s^{-1}}$$

the low-pressure limiting rate constants from an earlier work

$$k_{1,0}(N_2,T) = [N_2]\,(1.1 \pm 0.3) \times 10^{-30} (T/300\ \mathrm{K})^{-6.3\pm1.0}\ \mathrm{cm^3\ molecule^{-1}\ s^{-1}}$$

$$k_{1,0}(\mathrm{He},T) = [\mathrm{He}]\,(4.2 \pm 0.7) \times 10^{-31} (T/300\ \mathrm{K})^{-6.9\pm1.0}\ \mathrm{cm^3\ molecule^{-1}\ s^{-1}}$$

and theoretically estimated center-broadening factors

$$F_c(N_2) = 0.35 \pm 0.03\ (T/300\ \mathrm{K})^{-0.35}$$

$$F_c(\mathrm{He}) = 0.30 \pm 0.03\ (T/300\ \mathrm{K})^{-0.48}$$

which are consistent with the measurements, a full set of falloff curves can be constructed between 260 and 346 K.

Acknowledgment. Financial support of the work by the Deutsche Forschungsgemeinschaft (Sonderforschungsbereich 357 "Molekulare Mechanismen unimolekularer Prozesse") is gratefully acknowledged. K.O. thanks the Alexander von Humboldt Foundation for a fellowship. Helpful discussions with C. J. Cobos, J. Hahn, T. Lenzer, A. Maergoiz, J. Schroeder, H. Stark, and V. G. Ushakov are also acknowledged.

References and Notes

(1) Finlayson-Pitts, B. J.; Pitts, J. N., Jr. *Chemistry of the Upper and Lower Atmosphere: Theory, Experiments and Applications*; Academic Press: San Diego, CA, 2000.

(2) Seinfeld, J. H.; Pandis, S. N. *Atmospheric Chemistry and Physics: From air pollution to climate change*; Wiley: New York, 1998.

(3) Cobos, C. J.; Hippler, H.; Luther, K.; Ravishankara, A. R.; Troe, J. *J. Phys. Chem.* **1985**, *89*, 4332−4338.

(4) Troe, J. *J. Chem. Soc., Faraday Trans.* **1994**, *90*, 2303−2317.

(5) Pesa, M.; Pilling, M. J.; Robertson, S. H.; Wardlaw, D. M. *J. Phys. Chem. A* **1998**, *102*, 8526−8536.

(6) Fenter, F. F.; Lightfoot, P. D.; Niiranen, J. T.; Gutman, D. *J. Phys. Chem.* **1993**, *97*, 5313−5320.

(7) Danis, F.; Caralp, F.; Rayez, M. T.; Lesclaux, R. *J. Phys. Chem.* **1991**, *95*, 7300−7307.

(8) Nottingham, W. C.; Rudolph, R. N.; Andrews, K. P.; Moore, J. H.; Tossell, J. A. *Int. J. Chem. Kinet.* **1994**, *26*, 749−756.

(9) Ryan, K. R.; Plumb, I. C. *Int. J. Chem. Kinet.* **1984**, *16*, 591−602.

(10) Cooper, R.; Cumming, J. B.; Gordon, S.; Mulac, W. A. *Radiat. Phys. Chem.* **1980**, *16*, 169−174.

(11) Russell, J. J.; Seetula, J. A.; Gutman, D.; Danis, F.; Caralp, F.; Lightfoot, P. D.; Lesclaux, R.; Melius, C. F.; Senkan, S. M. *J. Phys. Chem.* **1990**, *94*, 3277−3283.

(12) Hippler, H.; Siefke, M.; Stark, H.; Troe, J. *Phys. Chem. Chem. Phys.* **1999**, *1*, 57−61.
(13) Lee, Y. R.; Tzeng, W. B.; Yang, Y. J.; Lin, Y. Y.; Lin, S. M. *Chem. Phys. Lett.* **1994**, *222*, 141−145.
(14) Lee, Y. R.; Yang, Y. J.; Lin, Y. Y.; Lin, S. M. *J. Chem. Phys.* **1995**, *103*, 6966−6972.
(15) Ryan, K. R.; Plumb, I. C. *J. Phys. Chem.* **1982**, *86*, 4678.
(16) Luther, K.; Oum, K.; Troe, J. Unpublished work.
(17) Blake, J. A.; Browne, R. J.; Burns, G. *J. Chem. Phys.* **1970**, *53*, 3320−3323.
(18) Danis, F.; Caralp, F.; Veyret, B.; Loirat, H.; Lesclaux, R. *Int. J. Chem. Kinet.* **1989**, *21*, 715−727.
(19) Ellermann, T. *Chem. Phys. Lett.* **1992**, *189*, 175−181.
(20) Catoire, V.; Lesclaux, R.; Schneider, W. F.; Wallington, T. J. *J. Phys. Chem.* **1996**, *100*, 14356−14371.
(21) Troe, J. *J. Phys. Chem.* **1979**, *83*, 114−126.
(22) Troe, J. *Ber. Bunsen-Ges. Phys. Chem.* **1983**, *87*, 161−169.
(23) Gilbert, R. G.; Luther, K.; Troe, J. *Ber. Bunsen-Ges. Phys. Chem.* **1983**, *87*, 169−177.
(24) Atkinson, R.; Baulch, D. L.; Cox, R. A.; Hampson, R. F., Jr.; Kerr, J. A.; Rossi, M. J.; Troe, J. *J. Phys. Chem. Ref. Data* **1997**, *26*, 521−1011.
(25) DeMore, W. B.; Sander, S. P.; Golden, D. M.; Hampson, R. F., Jr.; Kurylo, M. J.; Howard, C. J.; Ravishankara, A. R.; Kolb, C. E.; Molina, M. J. *JPL Publ.* **1997**, *97*−*4*.
(26) Maergoiz, A. I.; Nikitin, E. E.; Troe, J.; Ushakov, V. G. *J. Chem. Phys.* **1998**, *108*, 9987−9998.
(27) Troe, J. *J. Chem. Phys.* **1977**, *66*, 4745−4757.
(28) Troe, J. *J. Chem. Phys.* **1977**, *66*, 4758−4775.
(29) Forst, W.; Caralp, F. *J. Chem. Soc., Faraday Trans.* **1991**, *87*, 2307−2315.
(30) Otto, B.; Schroeder, J.; Troe, J. *J. Chem. Phys.* **1984**, *81*, 202−213.
(31) Troe, J. *J. Phys. Chem.* **1986**, *90*, 357−365.
(32) Hippler, H.; Schubert, V.; Troe, J. *Ber. Bunsen-Ges. Phys. Chem.* **1985**, *89*, 760−763.
(33) Reid, R. C.; Prausnitz, J. M.; Sherwood, T. K. *The Properties of Gases and Liquids*, 3rd ed.; McGraw-Hill: New York, 1977.
(34) (a) Okamoto, K.; Hirota, N.; Terazima, M. *J. Phys. Chem. A* **1997**, *101*, 5269−5277. (b) Terazima, M. *Acc. Chem. Res.* **2000**, *33*, 687−694.
(35) Ukai, A.; Hirota, N.; Terazima, M. *Chem. Phys. Lett.* **2000**, *319*, 427−433.
(36) Morita, A.; Kato, S. *J. Chem. Phys.* **1998**, *108*, 6809−6818.